International Journal of Nanomedicine

Dovepress
open access to scientific and medical research

Open Access Full Text Article

ORIGINAL RESEARCH

Nano-Scaled Zeolitic Imidazole Framework-8 as an Efficient Carrier for the Intracellular Delivery of RNase A in Cancer Treatment

This article was published in the following Dove Press journal:
International Journal of Nanomedicine

Jiaxin Jia
Shudi Zhang
Kai Wen
Quanshun Li

Key Laboratory for Molecular Enzymology and Engineering of Ministry of Education, School of Life Sciences, Jilin University, Changchun 130012, People's Republic of China

Background: Zeolitic imidazole framework-8 (ZIF-8) as an emerging platform has exhibited great potential in the protein delivery owing to its tunable chemical functionality.

Materials and methods: ZIF-8 was employed as a carrier for the encapsulation and intracellular delivery of RNase A, aimed to achieve a rapid release of proteins in an acidic environment. The intracellular uptake of RNase A was studied by confocal laser scanning microscopy (CLSM), and the inhibition of cell proliferation after the delivery of RNase A was evaluated by MTT assay, Live/Dead staining, and TUNEL cell apoptosis analysis, using human lung adenocarcinoma cell line A549 as a model. The biocompatibility of RNase A@ZIF-8 nanoparticles was systematically detected through the hemolysis and cytotoxicity assay.

Results: The RNase A@ZIF-8 nanoparticles constructed by biomimetic mineralization could not only facilitate the encapsulation of protein molecules (protein loading: 13.4%) but also maintain the enzymatic activity and stability of RNase A. The CLSM images showed that RNase A@ZIF-8 nanoparticles could efficiently improve the intracellular uptake of RNase A. Moreover, RNase A@ZIF-8 nanoparticles could obviously inhibit the cell proliferation through the induction of cell apoptosis, with 31.3% of cell death at an RNase A concentration of 10 μg/mL. Finally, RNase A@ZIF-8 nanoparticles were elucidated to possess excellent biocompatibility, with hemolysis of <5% using the same concentration of RNase A@ZIF-8.

Conclusion: ZIF-8 could be used as an effective carrier to deliver the therapeutic protein RNase A into the cytosol, which will be beneficial for improving the efficacy of cancer treatment.

Keywords: zeolitic imidazole framework-8, RNase A, biomimetic mineralization, protein delivery, metal-organic frameworks

Introduction

A class of therapeutic proteins with intracellular targets, including ribonuclease A (RNase A), Granzyme B, and caspase 3, have exhibited favorable ability to inhibit the proliferation of cancer cells, and thus they are of great significance in the treatment of malignancies.[1–4] For example, the cytotoxic RNase A could realize the cleavage of the intracellular RNA molecules and induce the apoptosis of tumor cells.[5–7] However, the clinical applications of protein-based drugs are strictly hindered by several factors, such as the rapid clearance by the immune system and enzymatic environment, and the poor cellular uptake efficiency.[8,9] To solve these problems, nano-scaled delivery systems including liposomes, cationic polymers, and inorganic nanoparticles have been

Correspondence: Quanshun Li
Tel +86-431-85155201
Fax +86-431-85155200
Email quanshun@jlu.edu.cn

submit your manuscript | www.dovepress.com
DovePress
http://doi.org/10.2147/IJN.S210107

successfully developed to circumvent the stability constraints and improve the intracellular delivery efficiency.[10–12]

Metal-organic frameworks (MOFs) are a type of well-regulated crystalline materials constructed by the coordination of metal ions and organic linkers, possessing unique properties such as tunable and uniform shape, precise pore size, and excellent physical and chemical stability.[13,14] Due to these characteristics, MOFs have been increasingly used as an indispensable tool to achieve the application in drug delivery.[15,16] Particularly, zeolite imidazole frameworks-8 (ZIF-8) assembled by zinc ion and 2-methylimidazole exhibits dodecahedral structure with high porosity and large surface area, which will be beneficial for the encapsulation of proteins.[17,18] Moreover, it has been reported to possess favorable biodegradability and low cytotoxicity, which makes it an attractive carrier in the drug or gene delivery.[19,20] Recently, ZIF-8 was demonstrated to be stable in the neutral conditions, but it was easily degraded in the acidic environment, revealing that the controlled drug release could be obtained in a pH-responsive manner.[21,22] In our previous report, a thermophilic lipase was successfully embedded into ZIF-8 through the biomimetic mineralization strategy, and the lipase@ZIF-8 composite possessed favorable catalytic activity and stability in the hydrolysis of esters and the kinetic resolution of *sec*-alcohols under harsh reaction conditions.[22] Therefore, ZIF-8 is anticipated to be an efficient carrier for facilitating the protein delivery and further realizing the protein-based cancer treatment.

Herein, ZIF-8 crystalline was synthesized as a protein carrier for the cancer treatment, where RNase A was employed as a model protein to evaluate the encapsulation efficiency and release profile (Scheme 1). The cellular uptake of RNase A@ZIF-8 nanoparticles was detected through confocal laser scanning microscopy (CLSM), and the inhibition of cell proliferation was evaluated using human lung adenocarcinoma cell line A549 as a model.

Materials and Methods

Materials

Bovine pancreatic RNase A, zinc acetate, 2-methylimidazole, and fluorescein isothiocyanate (FITC) were purchased from Sigma-Aldrich (St. Louis, MO, USA). Enzymatic activity was detected by RNase Alert® kit, which was obtained from Integrated DNA Technologies, Inc. (Coralville, IA, USA). BCA protein assay kit was obtained from BioTeke (Beijing, China). The LIVE/DEAD® Viability/Cytotoxicity kit was provided by ThermoFisher (Grand Island, NE, USA). One-step TUNEL cell apoptosis detection kit (green fluorescence) and lactate dehydrogenase (LDH) cytotoxicity assay kit were purchased from Beyotime (Jiangsu, China). Fetal bovine serum (FBS) and Dulbecco's modified Eagle's medium (DMEM) were purchased from Kangyuan Co. (Beijing, China) and Gibco (Grand Island, NE, USA), respectively. 3-(4,5-Dimethylthiazol-2-yl)-2,5-diphenyltetrazolium bromide (MTT) and 4′,6-diamidino-2-phenylindole (DAPI) were purchased from Amersco (Solon, OH, USA). All other reagents were of the highest grade available and used as received.

Construction of RNase A@ZIF-8 Nanoparticles

Briefly, 2-methylimidazole solution (160 mM) was added dropwise into 1 mL of RNase A solution (0.5 mg/mL), and zinc acetate solution (2 mL, 40 mM) and methanol (300

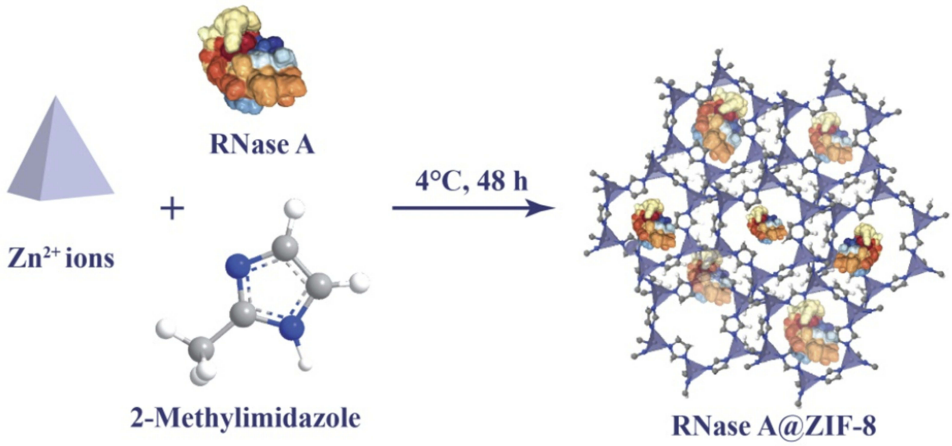

Scheme 1 The synthetic route of RNase A@ZIF-8 nanoparticles through biomimetic mineralization.

μL) were added into the mixture. After the incubation at 4° C for 48 hrs, the mixture was subjected to the centrifugation at 6000 r/min for 10 mins at 4°C to obtain RNase A@ZIF-8 nanoparticle, which was washed with distilled water three times and lyophilized as white powder. The protein loading in RNase A@ZIF-8 nanoparticles (%) was calculated according to the ratio of the total amount of loaded protein to the weight of nanoparticles, in which the protein concentration was measured by the BCA protein assay kit. The construction of FITC-RNase A@ZIF-8 nanoparticles was performed in a similar way as described above, where RNase A was replaced by FITC-labeled RNase A. For the synthesis of FITC-labeled RNase A, FITC (2.5 mg) and RNase A (5.0 mg) were dissolved in 10 mL of phosphate buffer saline (PBS, 50 mM, pH 8.0), and the mixture was stirred in a dark environment for 24 hrs, and FITC-labeled RNase A was purified through the ultrafiltration (MWCO: 8000 Da).

Characterization of RNase A@ZIF-8 Nanoparticles

The scanning electron microscopic (SEM) and transmission electron microscopic (TEM) images were observed through XL-30 ESEM FEG scanning electron microscope (FEI Company, USA) and JEM-2100F transmission electron microscope (JEOL, Japan), respectively. The elements mapping of RNase A@ZIF-8 nanoparticles was detected using energy dispersive spectrometer (EDS) attached to XL-30 ESEM FEG scanning electron microscope. Fourier Transform infrared spectroscope (FT-IR) was recorded in the range of 4000 to 600 cm^{-1} on a Bruker V70 Instrument (Bruker, Germany). The thermogravimetric analysis (TGA) was conducted on a TA Q500 thermal gravimetric analyzer (TA instrument, USA) at a heating rate of 10°C/min. The circular dichroism (CD) analysis was carried out on a JASCO J-810 spectrometer (JASCO Inc., Tokyo, Japan) with a scanning speed of 100 nm/min. The X-ray diffraction (XRD) analysis was performed on a Bruker D8 Advance (Bruker, Germany) with an acceleration voltage of 50 kV (200 mA, λ=1.54184 Å). Nitrogen adsorption and desorption experiments were conducted on a Micromeritics ASAP 2020 adsorptometer (Norcross, GA, USA), and the surface area of ZIF-8 and RNase A@ZIF-8 nanoparticles was determined through the Brunauer-Emmett-Teller (BET) method. The confocal fluorescence images were acquired by LSM 710 confocal laser scanning microscope (Carl Zeiss Microscopy LLC, Jena, Germany).

RNase A Release Profile of RNase A@ZIF-8

The RNase A@ZIF-8 nanoparticles were dispersed in PBS with pH values of 5.0, 6.0, and 7.0, respectively, in which 1 mg/mL of RNase A was used. The supernatant was collected by the centrifugation (6000 rpm, 15 min, 4 °C) at 2, 4, 6, 8, 10, and 12 hrs, and the protein concentration of supernatant was determined by BCA protein assay kit.

Cellular Uptake of RNase A@ZIF-8 Nanoparticles

The A549 cells were obtained from Shanghai Institute of Cell Bank (Shanghai, China) and cultured in DMEM medium supplemented with 10% FBS (pH value of 7.4) at 37° C under 5% CO_2, and all the pH values for the subsequent studies were set as 7.4. The cells were seeded into 6-well plates containing 2 mL DMEM medium and sterilized coverslips at a density of 1.5×10^5 cells/well and cultured overnight. The RNase A@ZIF-8 nanoparticles containing 10 μg/mL RNase A were then added into each well. After the incubation at 37°C for 6 hrs, the medium was discarded and the cells were washed with PBS three times. The cells were subsequently fixed with 4% paraformaldehyde solution for 20 mins and stained with DAPI solution (1 μg/mL) for 10 mins. Finally, the coverslips were rinsed with PBS three times and observed using LSM 710 confocal laser scanning microscope (Carl Zeiss Microscopy LLC, Jena, Germany).

Inhibition of Cell Proliferation

The A549 cells were seeded into 96-well plates containing 200 μL DMEM medium at a density of 5000 cells/well and incubated at 37°C overnight. The RNase A, ZIF-8 and RNase A@ZIF-8 nanoparticles containing different concentrations of RNase A were added into each well individually, and the cells were cultured for 48 hrs. For MTT assay, 20 μL of MTT solution (5 mg/mL) was added into each well and the cells were incubated for additional 4 hrs. The formed formazan was dissolved in 200 μL dimethyl sulfoxide (DMSO), and the absorbance at 570 nm was determined using HBS-1906A microplate reader (Nanjing, China). For LDH level in the medium, the absorbance at 490 nm was measured using the same microplate reader

after the cells were treated with LDH cytotoxicity assay kit according to the manufacturer's instructions.

Live/Dead Cell Staining Assay

The A549 cells were seeded in 6-well plates at a density of 1.5×10^5 cells/well and incubated at 37°C overnight. The cells were treated with free RNase A, ZIF-8, and RNase A@ZIF-8 nanoparticles harboring 10 μg/mL RNase A for 48 hrs. According to the manufacturer's instructions, the cells were treated with live/dead staining reagent for 30 mins, in which dead and viable cells were stained with ethidium homodimer and calcein AM, respectively.[23,24] After washing with PBS three times, the cells were observed through an IX71 fluorescence microscopy (Olympus, Tokyo, Japan).

TUNEL Cell Apoptosis Assay

The cell apoptosis was detected using TUNEL assay according to the previous report.[25] Briefly, the A549 cells were seeded in 6-well plates at a density of 1.5×10^5 cells/well and incubated overnight, and then treated with free RNase A, ZIF-8 and RNase A@ZIF-8 nanoparticles containing 10 μg/mL RNase A for 48 hrs. After washing with PBS twice, the cells were fixed with 1 mL of 4% paraformaldehyde solution for 30 mins and washed with PBS three times. According to the manufacturer's protocols, the cells were treated with PBS containing 0.1% Triton X-100 for 2 min and then incubated with TUNEL detection solution for 1 hr. Finally, the cell apoptosis was detected with IX71 fluorescence microscopy (Olympus, Tokyo, Japan).

Biocompatibility Analysis of RNase A@ZIF-8 Nanoparticles

The biocompatibility of RNase A@nanoparticles was assayed using the hemolysis of erythrocytes and cytotoxicity of L02 cells. For the hemolysis assay, the erythrocytes were collected from the fresh blood of Beagle dogs through the centrifugation at 1500 r/min for 10 mins. The cells were washed with PBS (pH=7.2) three times and suspended in PBS to a final concentration of 5.0×10^9 cells/mL. The stock suspension of erythrocytes (100 μL) was incubated with RNase A@ZIF-8 solution (900 μL) containing 10 μg/mL RNase A at 37 °C for 30 min. The samples were centrifuged at 1500 r/min for 10 min, and the absorbance at 578 nm was measured on a HBS-1906A microplate reader (Nanjing, China) to evaluate the hemolytic ability. The positive and negative controls were selected as the cells treated with 1% Triton X-100 and PBS, respectively. For the cytotoxicity analysis, human hepatocyte L02 cells obtained from Shanghai Institute of Cell Bank (Shanghai, China), were cultured and treated with different concentrations of RNase A@ZIF-8 nanoparticles, and then MTT assay was conducted as described above.

Statistical Analysis

Data were presented as mean value ± standard deviation (SD). One-way ANOVA test was used to calculate the statistical significance between different experimental groups and the control group (*$p < 0.05$; **$p < 0.01$, and ***$p < 0.001$).

Results and Discussion

Construction and Characterization of RNase A@ZIF-8 Nanoparticles

The synthesis procedure of RNase A@ZIF-8 nanoparticles in a biomimetic mineralization route was presented in Scheme 1. Briefly, zinc acetate solution was added into a mixture of 2-methylimidazole and RNase A at 4°C, and RNase A@ZIF-8 nanoparticles were obtained through the centrifugation after incubating for 48 hrs. The morphology and size of ZIF-8 and RNase A@ZIF-8 nanoparticles were studied through TEM and SEM analysis, as shown in Figure 1A and B. Clearly, both ZIF-8 and RNase A@ZIF-8 nanoparticles showed uniform dodecahedral structure, and RNase A@ZIF-8 nanoparticles exhibited an average diameter of 425.3 nm, which was larger than ZIF-8 (185.4 nm). These results were mainly caused by the successful loading of RNase A. However, the increased particle size was not favorable for the cellular uptake of nanoparticles. Thus, the cellular uptake and anti-proliferation of RNase A@ZIF-8 nanoparticles were systematically evaluated in the following studies. The XRD spectrum of RNase A@ZIF-8 nanoparticles exhibited a similar pattern to that of ZIF-8, demonstrating that the synthesis of RNase A@ZIF-8 nanoparticles did not alter the crystal structure of ZIF-8 (Figure 1C).

Further, a series of experiments were conducted to validate whether RNase A could be encapsulated in the ZIF-8 crystal. First, RNase A was replaced by FITC-labeled RNase A to construct the FITC-RNase A@ZIF-8 nanoparticles which were observed through CLSM. As shown in Figure 2A, strong fluorescence could be clearly observed in FITC-RNase A@ZIF-8 nanoparticles, revealing that FITC-labeled RNase A was successfully loaded in ZIF-8. Moreover, through the z-axis scanning, green fluorescence gradually increased from

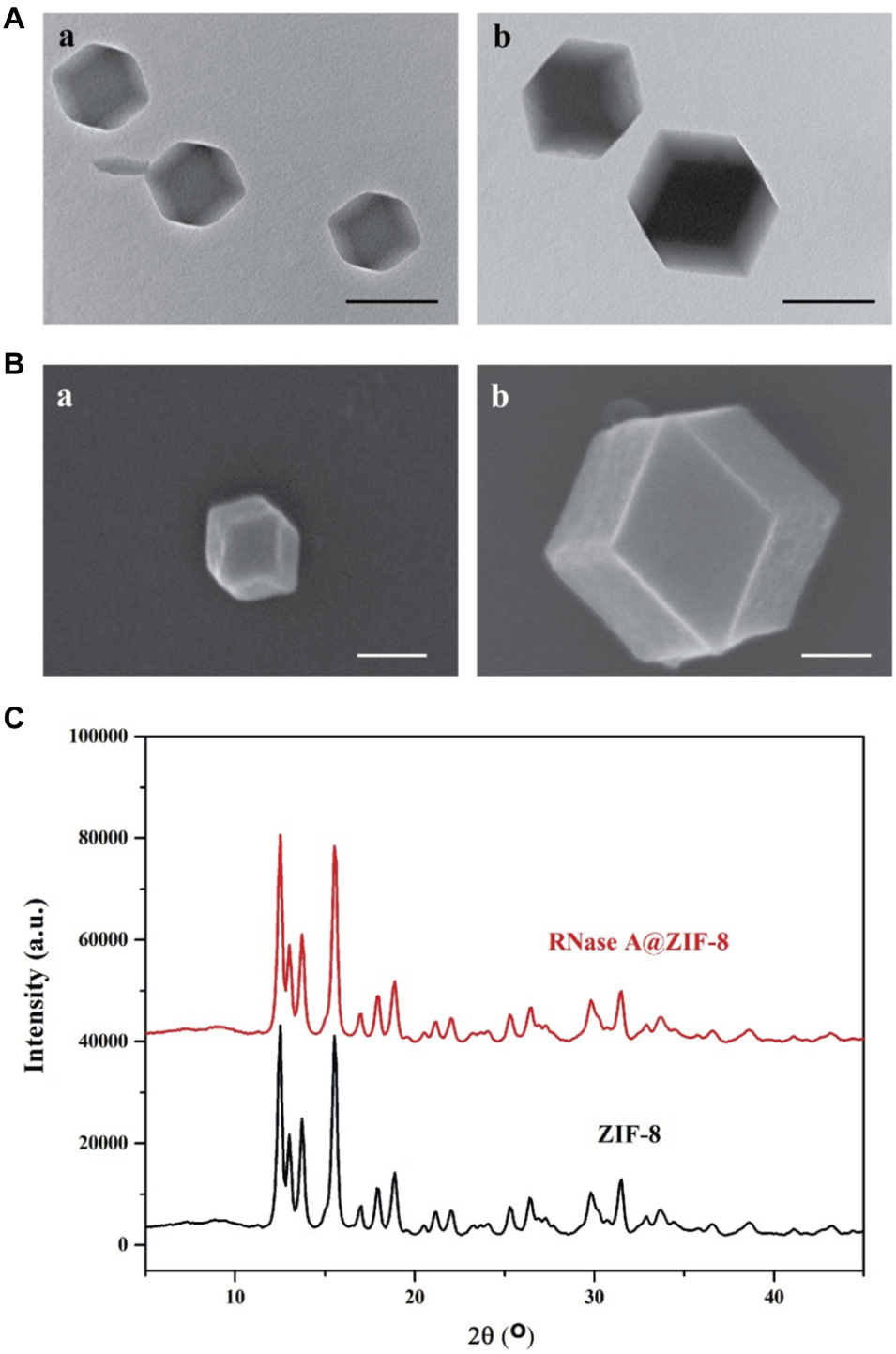

Figure 1 (**A**) The TEM images of ZIF-8 (a) and RNase A@ZIF-8 nanoparticles (b). Scale bar: 200 nm. (**B**) The SEM images of ZIF-8 (a) and RNase A@ZIF-8 nanoparticles (b). Scale bar: 200 nm. (**C**) The XRD pattern of ZIF-8 and RNase A@ZIF-8 nanoparticles.

the top to the middle and then decreased from the middle to the bottom, indicating that RNase A molecules could be embedded into the ZIF-8 crystal, not just adsorbed on the surface of ZIF-8 (Figure S1). Elements mapping analysis showed that compared to pure ZIF-8, an increasing amount of S element could be observed in RNase A@ZIF-8 nanoparticles which was attributed to the S signal of RNase A (Figures 2B and C, S2 and S3). These results were consistent with CLSM images, which also verified the successful encapsulation of RNase A in ZIF-8. In FT-IR spectrum of RNase A@ZIF-8 nanoparticles, characteristic bands at 1651 and 1570 cm^{-1} attributing to the amide bonds of RNase A and typical band at 756 cm^{-1}

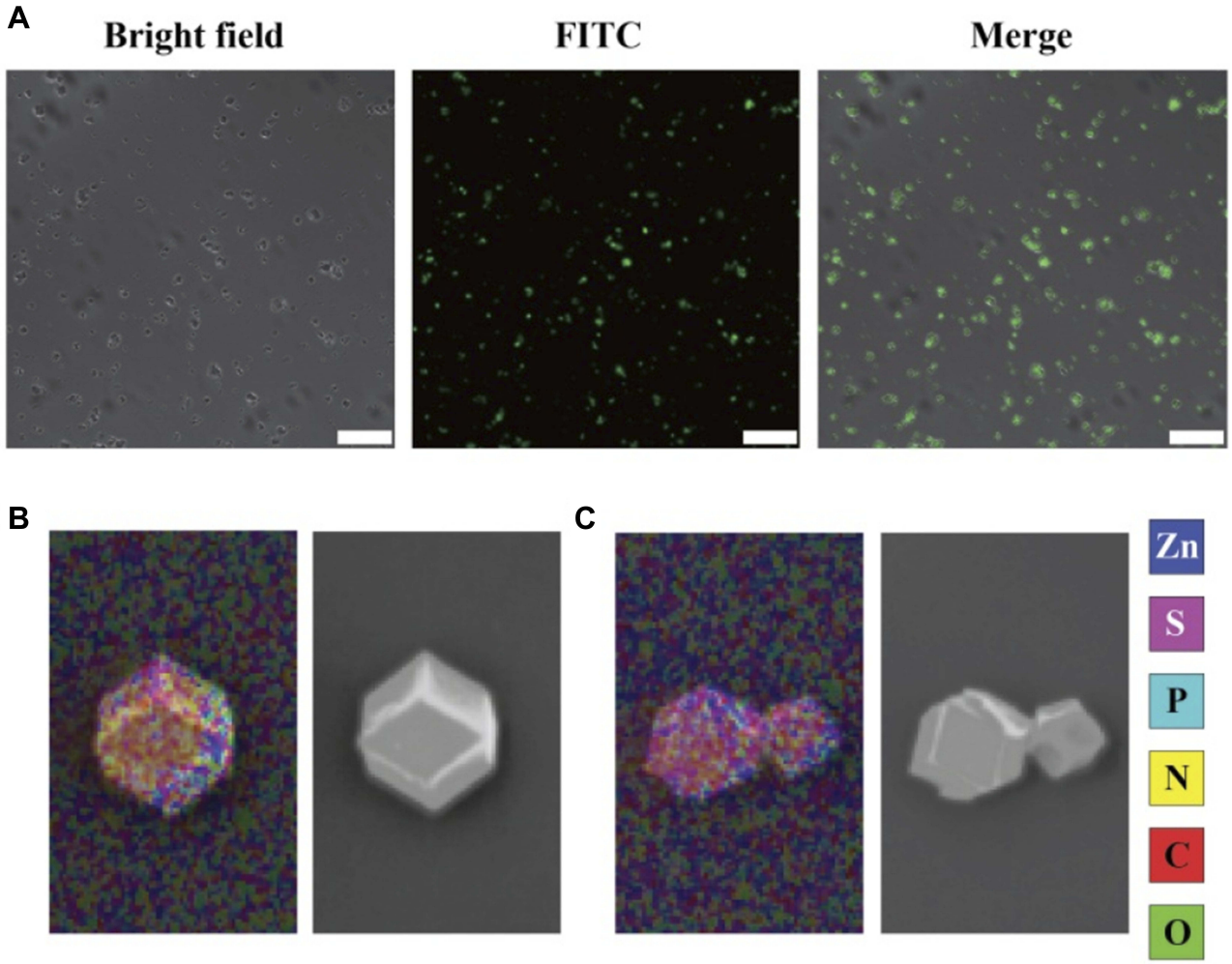

Figure 2 (**A**) The CLSM image of FITC-RNase A@ZIF-8 nanoparticles. Scale bar: 100 μm. (**B** and **C**) Elements mapping analysis of ZIF-8 and RNase A@ZIF-8 nanoparticles.

belonging to ZIF-8 could be clearly observed, indicating the presence of RNase A in the obtained nanoparticles (Figure 3A). In comparison to ZIF-8, TGA curve of RNase A@ZIF-8 nanoparticles achieved an improved weight loss in the temperature range of 200–400 °C (Figure 3B). These results were attributed to the removal of RNase A from RNase A@ZIF-8 nanoparticles, implying the existence of RNase A in the nanocomposite. The protein loading in RNase A@ZIF-8 nanoparticles was calculated to be 13.4% by BCA protein assay kit. Meanwhile, RNase A@ZIF-8 nanoparticles demonstrated a comparable enzymatic activity (90.77%) to the same amount of RNase A through RNase Alert® kit, indicating that the encapsulation of RNase A in ZIF-8 had almost no obvious influences on the enzymatic activity. After the complete removal of ZIF-8 crystal using the EDTA treatment, the secondary structure of RNase A was analyzed by CD spectra. As shown in Figure 3C, the RNase A component in RNase A@ZIF-8 nanoparticles still possessed a similar secondary structure to free RNase A, suggesting that the encapsulation in ZIF-8 did not trigger the structure changes of RNase A. In addition, the nitrogen adsorption-desorption curves in Figure 3D exhibited a typical type I isotherm, and the surface area of RNase A@ZIF-8 nanoparticles and pure ZIF-8 was calculated to be 523 and 613 m^2/g, respectively. These results suggested that RNase A molecules were indeed encapsulated into the ZIF-8 crystal.

In vitro RNase A Release Analysis

The coordination of zinc ions and organic ligand 2-methylimidazole in ZIF-8 could be easily disrupted in the acidic environment, leading to the release of cargos.[26–28] Thus, the in vitro release experiments were conducted in PBS solution with different pH values. As shown in Figure 4, the release of RNase A in RNase A@ZIF-8 nanoparticles could be achieved

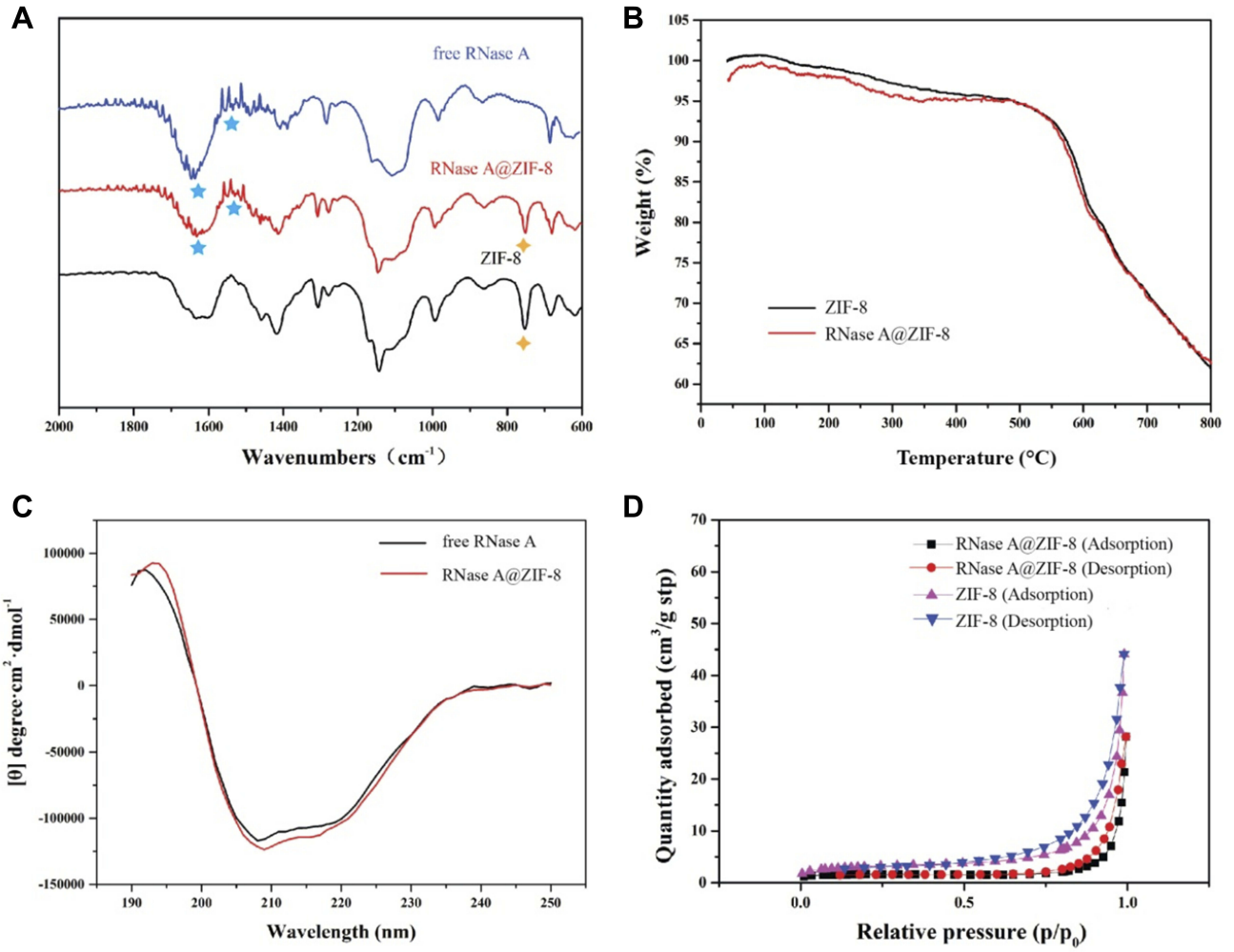

Figure 3 (**A**) The FT-IR spectra, (**B**) TGA curves, (**C**) CD spectra, and (**D**) nitrogen-adsorption-desorption isotherm curves of RNase A, ZIF-8 and RNase A@ZIF-8 nanoparticles.

with the elongation of time at all the pH conditions. Notably, it exhibited a relatively slower release under the pH of 7.0, where ca. 38.9% RNase A was released from the composites after 6 hrs. The release of RNase A in the neutral environment was probably caused by the interaction between Zn^{2+} and phosphate ions in PBS, thereby triggering the release of cargoes. In contrast, rapid release profiles could be obtained in the acidic environment, with 44.3% and 55.3% of RNase A released from RNase A@ZIF-8 nanoparticles after 6 hrs in pH 6.0 and 5.0, respectively. This results demonstrated that RNase A@ZIF-8 nanoparticles could achieve the protein release in a pH-responsive manner, thereby realizing the rapid release of RNase A in the acidic environment of tumors.

Cellular Uptake Assay

Efficient cellular uptake is always considered to be a critical step for the protein delivery,[29] and thus the endocytosis profile of RNase A@ZIF-8 nanoparticles was investigated through CLSM, using A549 cells as a model. As shown in Figure 5, almost no green fluorescence could be observed for free RNase A group due to the poor membrane impermeability of proteins. Remarkably, bright green fluorescence could be detected in the cells after the RNase A@ZIF-8 treatment, indicating that RNase A could be efficiently delivered into the cells with the aid of ZIF-8. To further detect whether RNase A@ZIF-8 nanoparticles were adsorbed on the cell surface, CLSM image with high resolution clearly demonstrated that FITC-labeled RNase A@ZIF-8 nanoparticles could enter the tumor cells (Figure S4). The results were mainly relied on the introduction of positively charged ZIF-8 which would facilitate the interaction between RNase A@ZIF-8 nanoparticles with the negatively charged cell membrane.

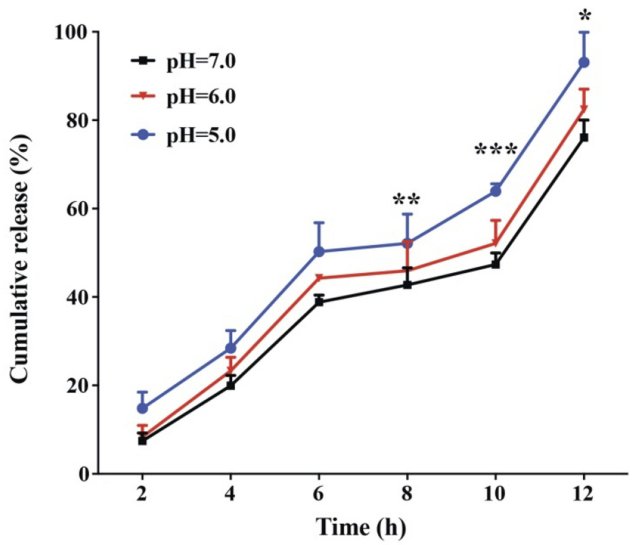

Figure 4 The RNase A release profile of RNase A@ZIF-8 in pH 5.0, 6.0 and 7.0, respectively. The data were expressed as mean value ± SD (*$p < 0.05$; **$p < 0.01$, and ***$p < 0.001$).

Anti-Proliferative Assay of RNase A@ZIF-8 Nanoparticles

After demonstrating the effective endocytosis of RNase A@ZIF-8, the anti-proliferation efficacy of nanoparticles was systematically investigated. The MTT assay showed that ZIF-8 exhibited limited cytotoxicity at the selected concentrations and free RNase A also had relatively weaker influence on the cell viability which was caused by the limited endocytosis ability of free enzyme (Figure 6A). Notably, compared with free RNase A, the RNase A@ZIF-8 nanoparticles could reduce the cell viability by 52.2% at an RNase A concentration of 10 μg/mL, indicating that RNase A@ZIF-8 nanoparticles could efficiently inhibit the proliferation of tumor cells owing to the successful cellular uptake and anti-proliferative function of RNase A. The IC_{50} values of RNase A and RNase A@ZIF-8 were measured to be 16.08 and 9.27 μg/mL, respectively, which elucidated the higher anti-proliferative ability of RNase A@ZIF-8 nanoparticles.

Further, the cell survival was evaluated through Live/Dead staining assay, in which the dead cells emitted red fluorescence after the staining with ethidium homodimer while the viable cells generated green fluorescence due to the calcein AM staining.[23,24] As shown in Figure S5, dead cells could barely be observed in free RNase A-treating group while a large number of dead cells could be clearly detected after the treatment with RNase A@ZIF-8 nanoparticles. In addition, the LDH release assay was conducted to quantify the cell death induced by RNase A@ZIF-8 nanoparticles, where LDH could be released into the medium after the damage of cell membrane. As shown in Figure 6B,

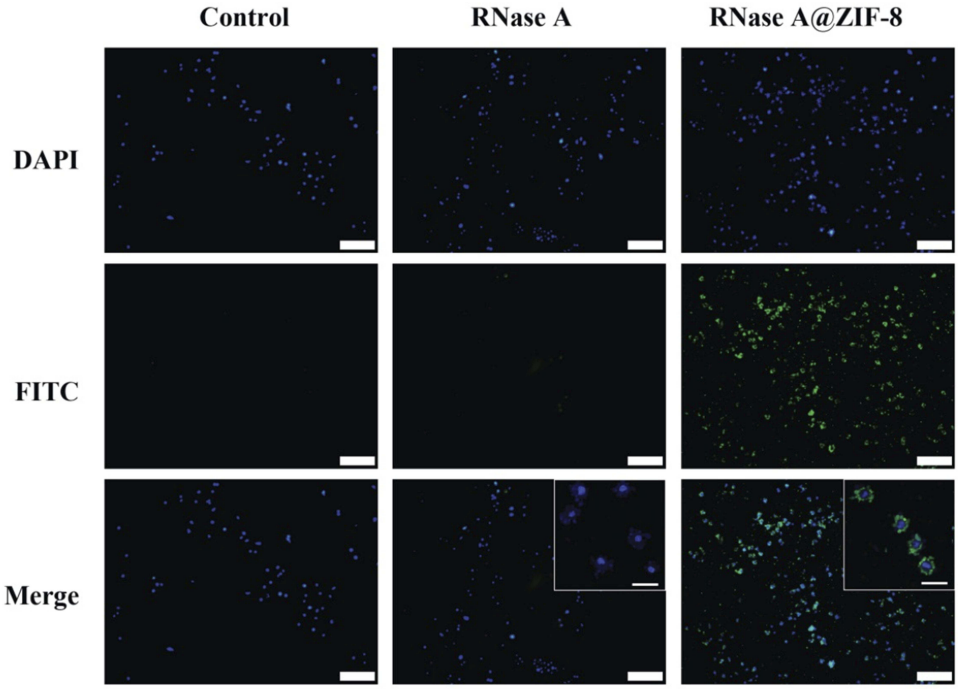

Figure 5 The cellular uptake of free FITC-labeled RNase A and FITC-RNase A@ZIF-8 nanoparticles. The images were acquired with 10 × magnification (scale bar: 100 μm), and the enlarged ones were obtained with 40 × magnification (scale bar: 20 μm).

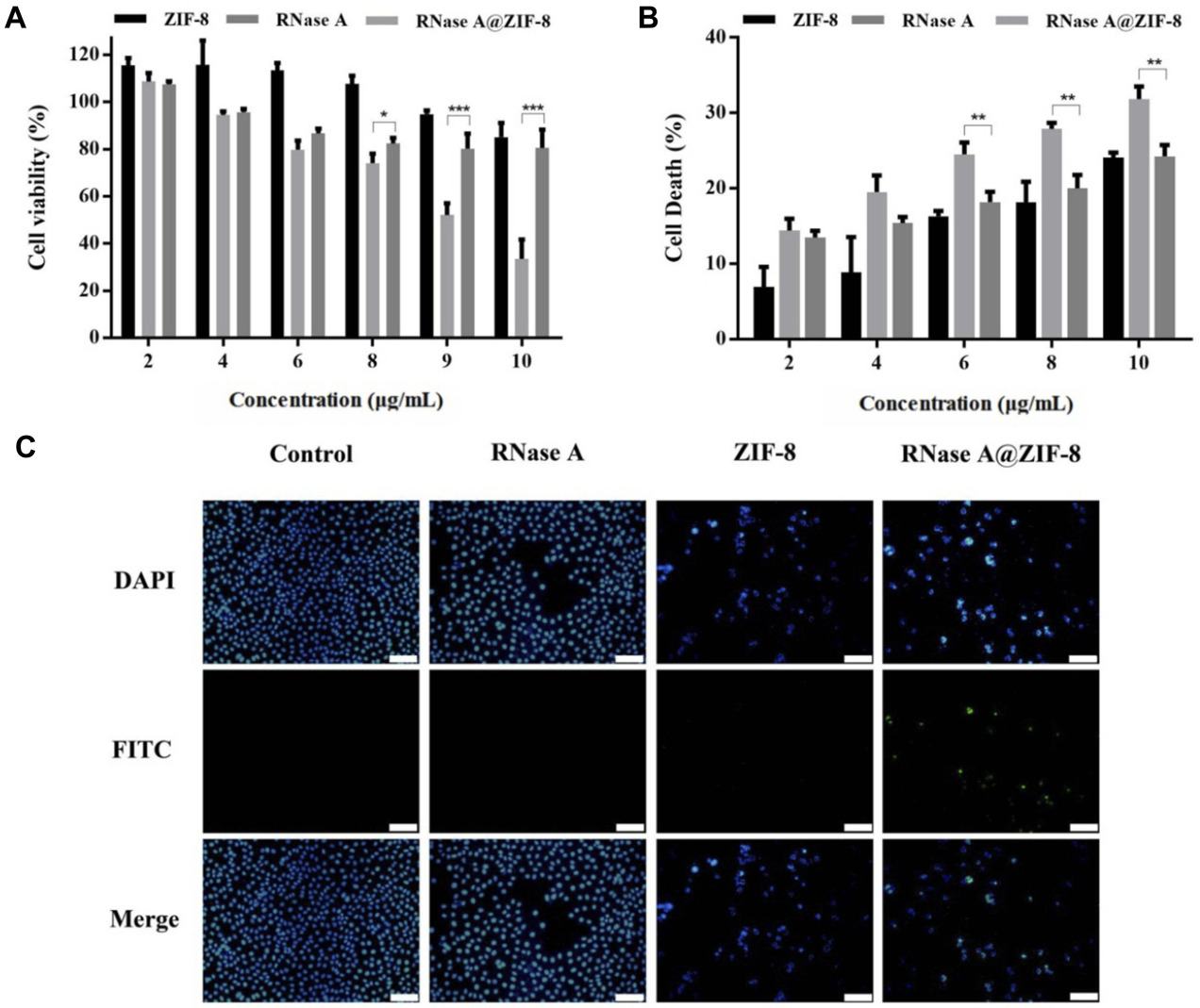

Figure 6 The anti-proliferative assay of RNase A@ZIF-8 nanoparticles against A549 cells through MTT (**A**), LDH release method (**B**), and TUNEL staining assay (**C**). The data were expressed as mean value ± SD (*$p < 0.05$; **$p < 0.01$, and ***$p < 0.001$). Scale bar: 50 μm.

RNase A@ZIF-8 nanoparticles could induce an obvious cell death in a concentration-dependent manner. Clearly, 31.3% of cell death could be achieved in the RNase A@ZIF-8-treating group at a concentration of 10 μg/mL, which was much higher than free RNase A with the same concentration. Moreover, TUNEL staining assay was performed to assess whether RNase A@ZIF-8 nanoparticles could induce the cell apoptosis which was a key factor in the inhibition of cell proliferation. As shown in Figure 6C, an increased green signal could be obtained in the cells treated with RNase A@ZIF-8 nanoparticles, indicating that RNase A@ZIF-8 nanoparticles could trigger the cell apoptosis. Thus, the anti-proliferative mechanism of RNase A@ZIF-8 nanoparticles was identified to be associated with the induction of cell apoptosis. Collectively, the results demonstrated that RNase A@ZIF-8 nanoparticles exhibited favorable inhibition ability on the cell proliferation, which was mainly caused by the fact that ZIF-8 could efficiently achieved the delivery of RNase A into tumor cells.

Biocompatibility Assay of RNase A@ZIF-8 Nanoparticles

Finally, the biocompatibility of RNase A@ZIF-8 was determined through hemolysis and MTT analysis, since the biocompatibility issues have become the major concerns in the current development of nanoparticles for biomedical applications. As shown in Figure 7, no hemolytic effect could be observed after the treatment of ZIF-8, whereas slight hemolysis was induced by the free RNase A treatment. In contrast,

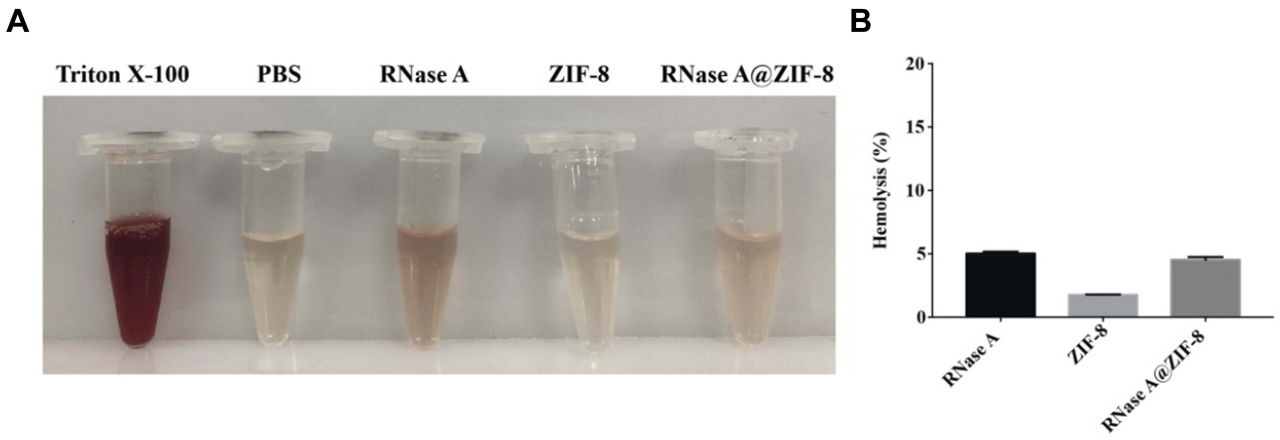

Figure 7 Visual observation (**A**) and hemolytic activity (**B**) of free RNase A, ZIF-8 and RNase A@ZIF-8 nanoparticles. The data were expressed as mean value ± SD.

compared with free RNase A, lower hemolysis was observed for the RNase A@ZIF-8 treatment group (hemolysis of <5%), indicating that ZIF-8 crystal could control the release of RNase A and prevent the interaction of embedded RNase A with the erythrocytes. Previous report has shown that materials with hemolysis (%) ranging from 2% to 5% were considered to be slight hemolysis and permissible for tissue engineering.[30] Thus, RNase A@ZIF-8 nanoparticles possessed favorable biocompatibility and did not induce the integrity disruption of erythrocyte membrane, providing a potential opportunity to conduct the in vivo anti-tumor evaluation. In addition, the biocompatibility of RNase A@ZIF-8 nanoparticles was evaluated through MTT assay, using normal cells L02 as a model. As shown in Figure S6, there were no obvious effects on the cell viability for these three groups, yielding >80% of cell viability at a high concentration of 10 μg/mL. Thus, RNase A@ZIF-8 nanoparticles possessed favorable biocompatibility in normal cells and will not cause serious side effects to normal tissues and organs.

Conclusion

In summary, we demonstrated that the nano-scaled ZIF-8 could be employed as a protein carrier for the intracellular delivery of RNase A. The RNase A@ZIF-8 nanoparticles could control the protein release in a pH-dependent manner, where the composite could achieve a rapid RNase A release in an acidic environment. Compared to free RNase A, ZIF-8 could obviously enhance the cellular uptake efficacy of RNase A. After the successful endocytosis by cancer cells, RNase A@ZIF-8 nanoparticles exhibited an in vitro anti-proliferative effect which was identified to be associated with the induction of cell apoptosis. Finally, RNase A@ZIF-8 nanoparticles showed an excellent biocompatible ability based on the hemolysis assay, which was beneficial for the future in vivo applications. Thus, RNase A@ZIF-8 obtained in a biomimetic mineralization manner could be considered to be a promising candidate for facilitating the delivery of therapeutic proteins and thus achieving the protein-based strategy in the clinic.

Acknowledgments

The authors gratefully acknowledge the supports from National Key R&D Program of China (2018YFC1105401), National Natural Science Foundation of China (81673502 and 81872928), Science & Technology Department of Jilin Province (20190201288JC), Education Department of Jilin Province (JJKH20190010KJ), Province-University Cooperation Project of Jilin Province (SXGJQY2017-4) and the Fundamental Research Funds of the Central Universities, China.

Disclosure

The authors report no conflicts of interest in this work.

References

1. Chen J, Ouyang J, Chen Q, et al. EGFR and CD44 dual-targeted multifunctional hyaluronic acid nanogels boost protein delivery to ovarian and breast cancers in vitro and in vivo. *ACS Appl Mater Interfaces*. 2017;9:24140–24147. doi:10.1021/acsami.7b06879
2. Shao D, Li M, Wang Z, et al. Bioinspired diselenide-bridged mesoporous silica nanoparticles for dual-responsive protein delivery. *Adv Mater*. 2018;30:1801198. doi:10.1002/adma.v30.29
3. Esteban-fernandez de Avila B, Ramirez-Herrera DE, Campuzano S, et al. Nanomotor-enabled pH-responsive intracellular delivery of caspase-3: toward rapid cell apoptosis. *ACS Nano*. 2017;11:5367–5374. doi:10.1021/acsnano.7b01926
4. Yang W, Wei Y, Yang L, et al. Granzyme B-loaded, cell-selective penetrating and reduction-responsive polymersomes effectively inhibit progression of orthotopic human lung tumor in vivo. *J Control Release*. 2018;290:141–149. doi:10.1016/j.jconrel.2018.10.013

5. Zhao S, Duan F, Liu S, et al. Efficient intracellular delivery of RNase A using DNA origami carriers. *ACS Appl Mater Interfaces*. 2019;11:11112–11118. doi:10.1021/acsami.8b21724
6. Nguyen DH, Lee JS, Choi JH, et al. Heparin nanogel-containing liposomes for intracellular RNase delivery. *Macromol Res*. 2015;23:765–769. doi:10.1007/s13233-015-3093-2
7. Liang X, Tang X, Yang J, et al. A genipin-crosslinked protein-polymer hybrid system for the intracellular delivery of ribonuclease A. *Int J Nanomed*. 2019;14:7389–7398. doi:10.2147/IJN.S210486
8. Yin L, Yuvienco C, Montclare JK. Protein based therapeutic delivery agents: contemporary developments and challenges. *Biomaterials*. 2017;134:91–116. doi:10.1016/j.biomaterials.2017.04.036
9. Rehman K, Akash SHM, Akhtar B, et al. Delivery of therapeutic proteins: challenges and strategies. *Curr Drug Targets*. 2016;17:1172–1188. doi:10.2174/1389450117666151209120139
10. Wang X, Li Y, Li Q, et al. Hyaluronic acid modification of RNase A and its intracellular delivery using lipid-like nanoparticles. *J Control Release*. 2017;263:39–45. doi:10.1016/j.jconrel.2017.01.037
11. Liu X, Zhang P, He D, et al. pH-reversible cationic RNase A conjugates for enhanced cellular delivery and tumor cell killing. *Biomacromolecules*. 2015;17:173–182. doi:10.1021/acs.biomac.5b01289
12. Cheng L, Yang L, Meng F, et al. Protein nanotherapeutics as an emerging modality for cancer therapy. *Adv Healthcare Mater*. 2018;7:1800685. doi:10.1002/adhm.v7.20
13. Wu M, Yang Y. Metal-organic framework (MOF)-based drug/cargo delivery and cancer therapy. *Adv Mater*. 2017;29:1606134. doi:10.1002/adma.201606134
14. Ibrahim M, Sabouni R, Husseini GA. Anti-cancer drug delivery using metal organic frameworks (MOFs). *Curr Med Chem*. 2017;24:193–214. doi:10.2174/0929867323666160926151216
15. Yang X, Tang Q, Jiang Y, et al. Nanoscale ATP-responsive zeolitic imidazole framework-90 as a general platform for cytosolic protein delivery and genome editing. *J Am Chem Soc*. 2019;141:3782–3786. doi:10.1021/jacs.8b11996
16. Lian X, Huang Y, Zhu Y, et al. Enzyme-MOF nanoreactor activates nontoxic paracetamol for cancer therapy. *Angew Chem Int Ed*. 2018;57:5725–5730. doi:10.1002/anie.201801378
17. Liedana N, Galve A, Rubio C, et al. CAF@ZIF-8: one-step encapsulation of caffeine in MOF. *ACS Appl Mater Interfaces*. 2012;4:5016–5021. doi:10.1021/am301365h
18. Liang K, Ricco R, Doherty CM, et al. Biomimetic mineralization of metal-organic frameworks as protective coatings for biomacromolecules. *Nat Commun*. 2015;6:7240. doi:10.1038/ncomms8240
19. Alsaiari SK, Patil S, Alyami M, et al. Endosomal escape and delivery of CRISPR/Cas9 genome editing machinery enabled by nanoscale zeolitic imidazolate framework. *J Am Chem Soc*. 2017;140:143–146. doi:10.1021/jacs.7b11754
20. Duan Y, Ye F, Huang Y, et al. One-pot synthesis of a metal-organic framework-based drug carrier for intelligent glucose-responsive insulin delivery. *Chem Commun*. 2018;54:5377–5380. doi:10.1039/C8CC02708K
21. Chen TT, Yi JT, Zhao YY, et al. Biomineralized metal-organic framework nanoparticles enable intracellular delivery and endo-lysosomal release of native active proteins. *J Am Chem Soc*. 2018;140:9912–9920. doi:10.1021/jacs.8b04457
22. Liang Z, Yang Z, Yuan H, et al. A protein@metal-organic framework nanocomposite for pH-triggered anticancer drug delivery. *Dalton Trans*. 2018;47:10223–10228. doi:10.1039/C8DT01789A
23. Wang Y, Chen J, Liang X, et al. An ATP-responsive codelivery system of doxorubicin and miR-34a to synergistically inhibit cell proliferation and migration. *Mol Pharm*. 2017;14:2323–2332. doi:10.1021/acs.molpharmaceut.7b00184
24. Dong M, Chen J, Zhang J, et al. A chemoenzymatically synthesized cholesterol-g-poly(amine-co-ester)-mediated p53 gene delivery for achieving antitumor efficacy in prostate cancer. *Int J Nanomed*. 2019;14:1149–1161. doi:10.2147/IJN.S191905
25. Kyrylkova K, Kyryachenko S, Leid M, et al. Detection of apoptosis by TUNEL assay. *Methods Mol Biol*. 2012;887:41–47. doi: 10.1007/978-1-61779-860-3_5
26. He H, Han H, Shi H, et al. Construction of thermophilic lipase-embedded metal-organic frameworks via biomimetic mineralization: a biocatalyst for ester hydrolysis and kinetic resolution. *ACS Appl Mater Interfaces*. 2016;8:24517–24524. doi:10.1021/acsami.6b05538
27. Jiang W, Wang X, Chen J, et al. Deuterohemin-peptide enzyme mimic-embedded metal-organic frameworks through biomimetic mineralization with efficient ATRP catalytic activity. *ACS Appl Mater Interfaces*. 2017;9:26948–26957. doi:10.1021/acsami.7b09218
28. Lyu F, Zhang Y, Zare RN, et al. One-pot synthesis of protein-embedded metal-organic frameworks with enhanced biological activities. *Nano Lett*. 2014;14:5761–5765. doi:10.1021/nl5026419
29. Sangsuwan R, Tachachartvanich P, Francis MB. Cytosolic delivery of proteins using amphiphilic polymers with 2-pyridinecarboxaldehyde groups for site-selective attachment. *J Am Soc Chem*. 2019;141:2376–2383. doi:10.1021/jacs.8b10947
30. Dang Q, Liu K, Liu C, et al. Preparation, characterization and evaluation of 3,6-O-N-acetylethylenediamine modified chitosan as potential antimicrobial wound dressing materials. *Carbohydr Polym*. 2018;180:1–12. doi:10.1016/j.carbpol.2017.10.019